

# Expert Insight-Enhanced Follow-up Chest X-Ray Summary Generation

Zhichuan Wang<sup>1,2</sup>[0009-0003-0373-3971], Kinhei Lee<sup>1</sup>[0009-0000-6832-9863], Qiao Deng<sup>1,2</sup>[0009-0004-6233-9840], Tiffany Y. So<sup>1</sup>[0000-0001-8268-0721], Wan Hang Chiu<sup>3</sup>[0000-0002-7930-1193], Yeung Yu Hui<sup>5</sup>[0000-0002-4887-7974], Bingjing Zhou<sup>1</sup>[0009-0007-9734-4721], and Edward S. Hui<sup>1,2,4</sup>✉[0000-0002-1761-0169]

<sup>1</sup> Department of Imaging and Interventional Radiology, the Chinese University of Hong Kong, Hong Kong, China

<sup>2</sup> CU Lab for AI in Radiology (CLAIR), The Chinese University of Hong Kong, HKSAR, China

<sup>3</sup> Hospital Authority, Hong Kong, China

<sup>4</sup> Department of Psychiatry, the Chinese University of Hong Kong, China

<sup>5</sup> China Unicom Global Limited  
edward.s.hui@gmail.com

**Abstract.** A chest X-ray radiology report describes abnormal findings not only from X-ray obtained at current examination, but also findings on disease progression or change in device placement with reference to the X-ray from previous examination. Majority of the efforts on automatic generation of radiology report pertain to reporting the former, but not the latter, type of findings. To the best of the authors' knowledge, there is only one work dedicated to generating summary of the latter findings, i.e., follow-up summary. In this study, we therefore propose a transformer-based framework to tackle this task. Motivated by our observations on the significance of medical lexicon on the fidelity of summary generation, we introduce two mechanisms to bestow expert insight to our model, namely expert soft guidance and masked entity modeling loss. The former mechanism employs a pretrained expert disease classifier to guide the presence level of specific abnormalities, while the latter directs the model's attention toward medical lexicon. Extensive experiments were conducted to demonstrate that the performance of our model is competitive with or exceeds the state-of-the-art.

**Keywords:** Follow-up chest X-ray · follow-up summary generation · multimodal representation learning.

## 1 Introduction

Chest X-ray radiology report generation can automatically report radiological findings on radiogram in an end-to-end manner [12,8], potentially providing a means to alleviate the workloads of radiologists. A major shortcoming of the majority of these models is that they are limited to reporting abnormalities in a given chest X-ray examination. Typically, radiologist writes reports not only

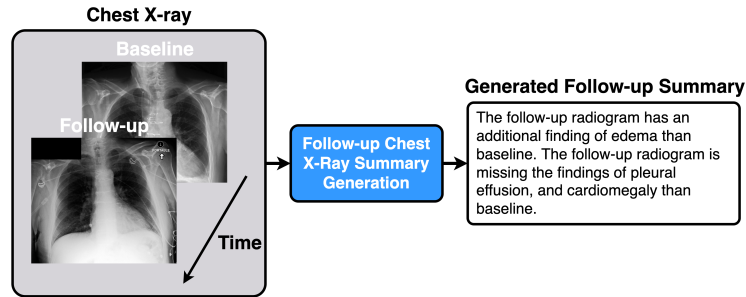


**Fig. 1.** A schematic of our proposed model that generates a textual summary of disease progression from a pair of chest X-rays taken at follow-up and baseline examinations.

based on a single (follow-up) X-ray examination but also by incorporating information from the X-ray from previous check-up to discern disease progression and/or change in device placement. Automatic generation of this type of report is known as follow-up report generation, a clinically critical yet largely understudied area. To the best of the knowledge, there is only one work [4] focusing on this field. We therefore aim to develop an end-to-end deep learning model to generate textual summary of disease progression from chest X-ray obtained at follow-up and baseline examinations (see Figure 1).

However, majority of the current models, namely follow-up summary generation [4], single radiogram report generation [12,8], or natural image difference caption [10,14], overlook the importance of meaningful entities, *i.e.*, the medical lexicon within the domain of follow-up summary generation. Specifically, these models typically generate a sentence word by word under the supervision of the masked language modeling loss. In this paradigm, these models pay equal attention to each word, which may not be optimal, as words related to abnormalities should deserve more attention than other words. This asymmetry results in a relatively lower accuracy in predicting abnormality-related words, thereby necessitating additional mechanism to improve the fidelity of follow-up summary generation.

Toward this end, we propose two mechanisms to bestow expert insight on follow-up chest X-ray summary generation, namely expert soft guidance and masked entity modeling loss. The former employs a pretrained expert disease classifier to provide complementary guidance on the presence level of certain diseases, while the latter directs the model’s attention toward abnormality-related words. Our contributions are:

- A framework is proposed to address the follow-up chest X-ray summary generation task, a clinically critical but largely understudied area.
- Two mechanisms, namely expert soft guidance and masked entity modeling loss, are proposed to bestow expert insight on disease-related words.
- Comprehensive experiments were conducted to demonstrate that the performance of our model is competitive with or exceeds the state-of-the-art.

## 2 Related Work

The work of Hu et al. [4] is arguably the inaugural work to tackle the task of follow-up summary generation. The authors have assembled a dataset, dubbed MIMIC-Diff-VQA, of radiogram pairs and their corresponding follow-up chest X-ray summaries using the MIMIC-CXR dataset [7]. They proposed EKAID, a graph-based network, to extract relationships between anatomical regions and diseases, with commendable performance.

The most related field in natural images is image difference caption, which aims to analyze the semantic differences in a given pair of images. The Spot-the-diff dataset was collected by [6] in 2018, marking the introduction of the image difference caption task. Later, Qiu et al. introduced a transformer-based model, MCCFormers, to capture the intra and inter-image relations, further improving the performance [10]. With the pretraining paradigm demonstrating a powerful ability in vision-language tasks, Yao et al. devised three pretraining tasks, IDCPCl, to align visual and textual features, achieving superior results compared to previous works [14].

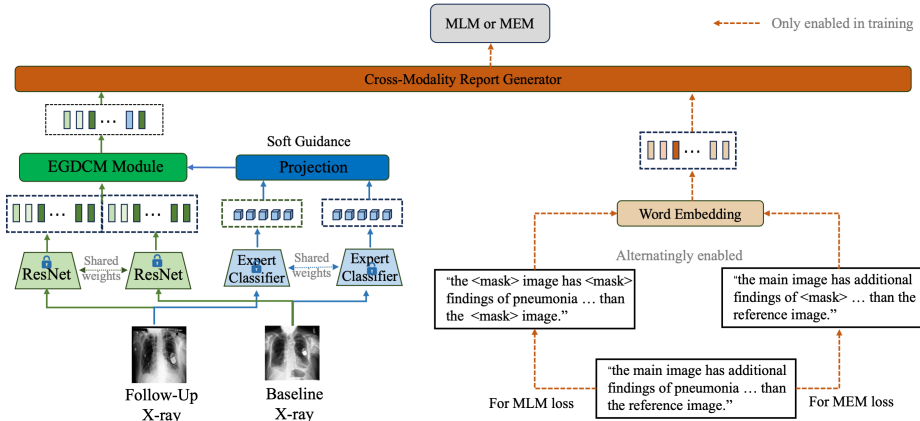


**Fig. 2.** Illustration of our proposed framework, expert insight-enhanced (EIE) follow-up chest X-ray summary generation. The dotted arrows indicate the branches that are only enabled in the training phase, and the symbol of lock indicates module that are frozen. EGDCM: expert guided difference capture module; MLM: masked language modelling; MEM: masked entity modelling.

## 3 Method

### 3.1 Preliminaries

Given an X-ray pair  $(\mathbf{I}^f, \mathbf{I}^b)$  from the same patient, where  $\mathbf{I}^f$  and  $\mathbf{I}^b$  respectively represent X-ray images obtained at follow-up and baseline examinations. Our

goal is to generate a summary of radiological findings  $\mathbf{s}$  that describes disease progression and/or change in device placement at the time of follow-up X-ray examination. Such summary is dubbed as follow-up summary from hereon.

During the training phase, X-ray pair  $\{(\mathbf{I}^f, \mathbf{I}^b)\}_{i \in \mathbb{D}}$  and the corresponding ground-truth follow-up summary  $\{\mathbf{s}^{(i)}\}_{i \in \mathbb{D}}$  from training dataset  $\mathbb{D}$  were used to train the model. Building upon prior research [14,10], every word in  $\mathbf{s}$  underwent tokenization and was subsequently mapped to word embeddings via an embedding layer initiated with training from the ground up. Three special tokens were added to facilitate the training process, namely [CLS], [BOS] and [EOS]. [CLS] was added to merge the information of all word tokens, and [BOS] and [EOS] were used to identify the beginning or ending of a sentence. The text input can be represented as:

$$\bar{\mathbf{s}} = ([\text{CLS}], [\text{BOS}], w_1, \dots, w_{N_s}, [\text{EOS}]), \quad (1)$$

where  $w_i$  represents the token of the  $i^{\text{th}}$  word in  $\mathbf{s}$ . Similar to the approach in [14], a pretrained ResNet101 [3] was adopted to obtain the image features from the X-ray pair, which were then flattened into a sequence of image tokens:

$$\mathbf{V}^b = ([\text{Xray1}], \mathbf{V}_0^b, \dots, \mathbf{V}_{N_v}^b), \quad \mathbf{V}^f = ([\text{Xray2}], \mathbf{V}_0^f, \dots, \mathbf{V}_{N_v}^f), \quad (2)$$

where [Xray1] and [Xray2] are two tokens for capturing the comprehensive representations of individual X-ray images, and  $\mathbf{V}_i^b$  and  $\mathbf{V}_i^f$  represent the  $i^{\text{th}}$  image token of the baseline and follow-up X-ray, respectively. Furthermore, fixed positional embeddings and type embeddings were incorporated, with the former designed to denote token positions and the latter employed to distinguish the source of a particular token, such as  $\mathbf{V}^f$ ,  $\mathbf{V}^b$ , or  $\bar{\mathbf{s}}$ .

### 3.2 Model Architecture

The overall architecture of our proposed model, expert insight-enhanced (EIE) follow-up chest X-ray summary generation, is illustrated in Figure 2. A pair of X-ray images are fed into a pretrained ResNet to extract image features, serving as image tokens after flattening. The same pair of X-ray are also input into a pretrained expert disease classifier to obtain the probability of the presence of certain diseases, which is then projected into the same dimension as image tokens. Image and soft-guidance tokens are fed into the transformer-based expert guided difference capture module (EGDCM) to obtain the difference representation. The output tokens of EGDCM and word tokens are input into the cross-modality summary generator to produce the follow-up chest X-ray summary. The generation is supervised by the masked language modeling (MLM) loss and masked entity modeling (MEM) loss.

**Expert Soft Guidance** To bestow expert insight to the model for enhancing the prediction of abnormality-related words, known as entities, complementary

guidance on the presence level of certain diseases was provided by a pretrained multi-class expert classifier.

Given an X-ray pair  $(\mathbf{I}^f, \mathbf{I}^b)$ , a pretrained multi-class disease classifier was employed to generate the probability of the presence of a number of abnormalities, denoted as  $(\mathbf{p}^f, \mathbf{p}^b)$ . Rather than using a hard threshold to binarize these probabilities, they were directly mapped into the same feature space of image tokens through a projection module. Subsequently, the guidance tokens were obtained and used to guide the expert guided difference capture module (EGDCM) in capturing a more disease-related representation. Formally, the process of obtaining the soft guidance can be denoted as:

$$\mathbf{p}^j = F_e(\mathbf{I}^j), \quad (3)$$

$$\mathbf{g}^j = \text{Proj}(\mathbf{p}^j) \quad \text{for } j \in \{f, b\}, \quad (4)$$

where  $F_e$  denotes the expert classifier,  $\text{Proj}(\cdot)$  denotes the projection layer, and  $\mathbf{g}^j$  represents the soft-guidance token. Similar to image tokens, the soft-guidance tokens  $\mathbf{g}^j$  are appended with fixed positional embeddings and type embeddings.

**Expert-Guided Difference Capture Module** We propose an expert-guided difference capture module (EGDCM)  $F_{\text{diff}}$  to extract the representations of the difference in the image features of two different examinations. To better model long-distance dependencies and merge information from image and texts, EGDCM is composed of a two-layer transformer, which takes all image tokens and guidance tokens as input. Formally, the process can be written as:

$$\mathbf{V}_E^b = ([\text{xray1}], \mathbf{V}_0^b, \dots, \mathbf{V}_{N_v}^b, \mathbf{g}^b), \quad \mathbf{V}_E^f = ([\text{xray2}], \mathbf{V}_0^f, \dots, \mathbf{V}_{N_v}^f, \mathbf{g}^f) \quad (5)$$

$$\{\bar{\mathbf{V}}^f, \bar{\mathbf{V}}^b\} = F_{\text{diff}}(\{\mathbf{V}_E^f, \mathbf{V}_E^b\}). \quad (6)$$

**Cross-Modality Follow-Up Summary Generator** A three-layer transformer was employed for the cross-modality report generator  $F_{\text{gen}}$ , which took the image difference tokens and summary tokens as inputs:

$$(\hat{\mathbf{V}}^f, \hat{\mathbf{V}}^b, \hat{\mathbf{s}}) = F_{\text{gen}}(\bar{\mathbf{V}}^f, \bar{\mathbf{V}}^b, \bar{\mathbf{s}}) \quad (7)$$

### 3.3 Loss Functions

To endow the model with the ability to generate follow-up chest X-ray summary, the widely used MLM loss [14,2] was adopted. Furthermore, we propose a new MEM loss, an extension of MLM, to enhance the prediction of the abnormality-related words.

**Masked Language Modeling Loss** In contrast to many vision-language pre-training works, the uni-directional MLM loss was employed to emulate the sentence generation process of inference. In other words, instead of considering all

Method	BLEU-1	BLEU-2	BLEU-3	BLEU-4	METEOR	ROUGE <sub>L</sub>	CIDEr	Acc5	Acc14
MCCFormers <sup>†</sup>	0.214	0.190	0.170	0.153	0.319	0.340	0.000	-	-
IDCPCL <sup>†</sup>	0.614	0.541	0.474	0.414	0.303	0.582	0.703	-	-
EKAID	0.628	0.553	0.491	0.434	0.339	0.577	1.027	68.21 <sup>‡</sup>	81.00 <sup>‡</sup>
EIE-base	0.574	0.510	0.456	0.407	0.416	0.590	0.968	59.94	77.57
EIE-mem	0.614	0.547	0.492	0.441	0.405	0.616	1.421	65.89	79.14
EIE-esg	0.638	0.573	0.519	0.469	0.399	0.636	1.615	68.33	81.63
EIE-all	0.646	0.583	0.528	0.477	0.401	0.635	1.698	70.98	81.47

**Table 1.** Comparison with State-of-the-Art (SOTA): **EIE-all** surpasses existing SOTA by a substantial margin across all metrics. Furthermore, each proposed mechanism notably enhances the performance of the base model. The combination of both mechanisms leads to further improvement. <sup>†</sup> Results were reported from EKAID. <sup>‡</sup> Results were reproduced using the official codes of EKAID.

text tokens, the prediction of the  $i^{th}$  (masked) word was based solely on its preceding words  $w_{<i}$  and other image-related tokens ( $\hat{\mathbf{V}}^f, \hat{\mathbf{V}}^b$ ). The same masking strategy as BERT [2] was used, where 15% of the input text tokens were randomly selected, with 80% of which masked by the special token [MASK], 10% substituted with words randomly chosen in vocabulary, and the remaining 10% left unchanged. To obtain the final predictions, the masked tokens were input into a linear classifier. Formally, the uni-directional MLM loss over  $\mathbb{D}$  can be written as:

$$L_{\text{MLM}} = \mathbb{E}_{\mathbb{D}}[-\log P_{\theta}(w_i|w_{<i}, \hat{\mathbf{V}}^f, \hat{\mathbf{V}}^b)] \quad \text{for } \forall i \in \{1, \dots, N_s\}, \quad (8)$$

where  $\theta$  is the trainable parameters of the model.

**Masked Entity Modeling Loss** Prediction of entities, can be enhanced by directing model’s attention toward these words through our proposed MEM. Masked entity modeling loss is formulated similar to the MLM loss, but with the masking of the selected entity words:

$$L_{\text{MEM}} = \mathbb{E}_{\mathcal{D}}[-\log P_{\theta}(w_i|w_{<i}, \hat{\mathbf{V}}^f, \hat{\mathbf{V}}^b)] \quad \text{for } w_i \in \mathcal{E}, \quad (9)$$

where  $\mathcal{E}$  is the selected entity set.

Given that expert soft guidance can only offer soft guidance for certain abnormalities, the MEM loss serves as a complement to expert soft guidance by enhancing the prediction of the remaining common and crucial abnormality-related words. For more details on entity selection, please refer to the appendix.

It is worth noting that, thanks to the parallel computation of transformer blocks, the soft guidance tokens  $\mathbf{g}^f$  and  $\mathbf{g}^b$  can be easily injected into or removed from the difference capturing process. When the model was trained solely with the MLM loss and without enabling expert soft guidance, we name the model as **EIE-base**. When **EIE-base** was combined with expert soft guidance or MEM loss, we refer to it as **EIE-esg** and **EIE-mem**, respectively. When **EIE-base** was combined with both proposed mechanisms, it is denoted as **EIE-all**.

### 3.4 Training Strategy

When both of the MLM and MEM losses were enabled, an alternating optimization strategy was adopted. Specifically, an enabling probability  $\alpha$  was assigned to the MEM loss. In a given training iteration, a random sample  $r$  was drawn from a uniform distribution between 0 and 1. The MEM loss was employed if  $r > \alpha$ ; the MLM loss was enabled otherwise. The optimization direction was controlled by adjusting the hyperparameter  $\alpha$ .

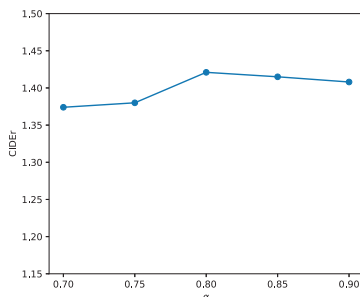


Fig. 3. Hyperparameter  $\alpha$  sensitivity study of EIE-mem.

## 4 Experiments

### 4.1 Dataset and Metrics

Our model was evaluated on the MIMIC-Diff-VQA [4] dataset, which contains 164,324 X-ray pairs and the corresponding follow-up reports. Following [4,14], widely used natural language generation metrics including BLEU [9], METEOR [1], ROUGE<sub>L</sub> [11] and CIDEr [13] were adopted to evaluate the model on summary generation. Following [8], our method was also evaluated using accuracy Acc5 and Acc14 to demonstrate its ability on abnormality recognition, where Acc5 denotes the micro average accuracy over 5 most common abnormalities and Acc14 is that over 14 abnormalities of CheXpert [5]. Please refer to the appendix for more details on the abnormalities, the metrics and their computation.

### 4.2 Implementation Details

Consistent with previous works [14], a pretrained ResNet101 was employed to extract grid features with a shape of (7, 7, 1024), which were then flattened into a sequence of image tokens with a shape of (49, 1024). For all transformer-based modules, the hidden feature size was 512, the number of multi-heads was 8, and the layer numbers were 2 and 3 for the EGDCM and cross-modality follow-up summary generator, respectively. The word embedding layers were learnt from

Threshold	BLEU1	BLEU2	BLEU3	BLEU4	METEOR	ROUGE <sub>L</sub>	CIDEr
0.4	0.548	0.491	0.445	0.403	0.304	0.511	1.557
0.5	0.578	0.517	0.470	0.426	0.317	0.523	1.579
0.6	0.571	0.511	0.464	0.421	0.314	0.520	1.576
Soft guidance	0.638	0.573	0.519	0.469	0.399	0.636	1.615

**Table 2.** Comparison with hard versus soft guidance.

scratch, and the feature dimension was set to 512. The hyperparameter  $\alpha$  in the alternating optimization strategy was set to 0.8. The Adam optimizer was used with a learning rate of  $3e-5$ , and the total training iteration was set to 100k. Our expert classifier was based on PCAM [15]. For more details, please refer to the appendix.

### 4.3 Comparison with the State-of-the-Art

As depicted in Table 1, with the exception of the **EIE-base** model, other versions of the proposed methods outperformed existing SOTA by a considerable margin, with **EIE-all** achieving the best performance. Taking **EIE-all** as an example, there were improvements of 1.8%, 3.0%, 3.7%, and 4.3% on the BLEU metrics. For METEOR, a performance gain up to 6.2% was achieved. The increase was more pronounced on ROUGE<sub>L</sub> and CIDEr, with **EIE-all** boosting the performance by 5.8% and 0.671, respectively. The relative increase in CIDEr was particularly large, at 65.3% compared with EKAID. For Acc5 and Acc14, a 2.77% and 0.47% accuracy performance gain was obtained. These results demonstrate that our method performs better on both the report level and the clinical level.

### 4.4 Ablation Study

As illustrated in Table 1, each proposed mechanism notably enhanced the performance of our base model, both at the generation and clinical levels. **EIE-mem** achieved improvements of 4.0%, 3.7%, 3.6%, and 3.4% on the BLEU metric, with a 2.6% and 0.453 increase in ROUGE<sub>L</sub> and CIDEr, respectively. There were improvements in both Acc5 and Acc14, at 5.95% and 1.57% respectively. For **EIE-esg**, the performance gains were 6.4%, 6.3%, 6.3%, and 6.2% on BLEU, 8.39% on Acc5, and 4.06% on Acc14. ROUGE<sub>L</sub> increased from 59.0% to 63.6%, and CIDEr increased from 0.968 to 1.615. Notably, the relative increase in CIDEr was 66.84%. Combining the MEM loss and expert soft guidance further improved performance, with **EIE-all** achieving gains of 7.2%, 7.3%, 7.2%, 7.0%, 4.5%, 0.73, 11.04%, and 3.9% on BLEU, ROUGE<sub>L</sub>, CIDEr, Acc5, and Acc14 respectively.

### 4.5 Hyper-Parameter Sensitivity Study

Several experiments were conducted to analyze how the performance of **EIE-mem** varied with the hyper-parameter  $\alpha$ , which controls the enable probability



of the MEM loss. The results are presented in Figure 3. The CIDEr score ranged from 1.37 to 1.42, and surpassed 1.027, which was that of the existing state-of-the-art[4]. The best result of 1.42 was obtained when  $\alpha = 0.8$ . Consequently, we set  $\alpha$  to 0.8 in all experiments.

#### 4.6 Comparison with Hard Guidance

Several experiments were conducted to compare the performance of hard guidance with that of soft guidance. To obtain hard guidance, a sigmoid function was applied to the output of the expert classifier, which was subsequently binarized using a threshold. The results are presented in Table 2. Soft guidance outperformed hard guidance, particularly in METEOR and ROUGE<sub>L</sub> metrics. Setting the threshold at 0.5 yields the best results among all hard guidance experiments. Soft guidance achieved 6.0%, 5.6%, 4.9%, and 4.3% improvement in BLEU metric, 8.2% in METEOR, 11.3% in ROUGE<sub>L</sub>, and 0.036 in CIDEr. The relative performance increases in METEOR and ROUGE<sub>L</sub> were 25.87% and 21.6%, respectively. These experiments affirm that soft guidance is more effective and robust, as it eliminates the need for careful hyperparameter selection.

#### 4.7 Lightweight EIE-all and more experiments

In addition to the aforementioned experiments, the appendix contains supplementary experimental results and showcases, including a lightweight version of **EIE-all**. This variant utilized expert guidance during the training phase to enhance the knowledge learning, whilst omitting the expert soft guidance branch during inference. In addition, the performance of a model with a stronger and recently proposed expert classifier was also investigated, indicating that model performance can be further improved with better expert guidance. For more details, please refer to the appendix.

### 5 Limitations

Albeit exceeding the performance of SOTA, our proposed model warrants further improvement in its clinical accuracy. In addition, we will bestow our model the ability to predict the location of abnormalities in future studies.

### 6 Conclusion

A transformer-based framework was proposed to address the clinically critical yet largely understudied task of follow-up chest X-ray summary generation. Two mechanisms, namely expert soft guidance and masked entity modeling loss, were proposed to bestow expert insight on abnormality recognition for improving the overall model performance. Extensive experiments demonstrated that the performance of our model is competitive with or exceeds the state-of-the-art.

## References

1. Denkowski, M., Lavie, A.: Meteor universal: Language specific translation evaluation for any target language. In: Proceedings of the ninth workshop on statistical machine translation. pp. 376–380 (2014)
2. Devlin, J., Chang, M.W., Lee, K., Toutanova, K.: Bert: Pre-training of deep bidirectional transformers for language understanding. arXiv preprint arXiv:1810.04805 (2018)
3. He, K., Zhang, X., Ren, S., Sun, J.: Deep residual learning for image recognition. In: Proceedings of the IEEE conference on computer vision and pattern recognition. pp. 770–778 (2016)
4. Hu, X., Gu, L., An, Q., Zhang, M., Liu, Liangchen, e.: Expert knowledge-aware image difference graph representation learning for difference-aware medical visual question answering. In: Proceedings of the 29th ACM SIGKDD Conference on Knowledge Discovery and Data Mining. pp. 4156–4165 (2023)
5. Irvin, J., Rajpurkar, P., Ko, M., Yu, Y., Ciurea-Ilcus, S., Chute, C., Marklund, H., Haghighi, B., Ball, R., Shpanskaya, K., et al.: Chexpert: A large chest radiograph dataset with uncertainty labels and expert comparison. In: Proceedings of the AAAI conference on artificial intelligence. vol. 33, pp. 590–597 (2019)
6. Jhamtani, H., Berg-Kirkpatrick, T.: Learning to describe differences between pairs of similar images. arXiv preprint arXiv:1808.10584 (2018)
7. Johnson, A.E., Pollard, T.J., Berkowitz, S.J., Greenbaum, N.R., Lungren, M.P., Deng, C.y., Mark, R.G., Horng, S.: MIMIC-CXR, a de-identified publicly available database of chest radiographs with free-text reports. *Scientific data* **6**(1), 317 (2019)
8. Miura, Y., Zhang, Y., Tsai, E.B., Langlotz, C.P., Jurafsky, D.: Improving factual completeness and consistency of image-to-text radiology report generation. arXiv preprint arXiv:2010.10042 (2020)
9. Papineni, K., Roukos, S., Ward, T., Zhu, W.J.: Bleu: a method for automatic evaluation of machine translation. In: Proceedings of the 40th annual meeting of the Association for Computational Linguistics. pp. 311–318 (2002)
10. Qiu, Y., Yamamoto, S., Nakashima, K., Suzuki, R., Iwata, K., Kataoka, H., Satoh, Y.: Describing and localizing multiple changes with transformers. In: Proceedings of the IEEE/CVF International Conference on Computer Vision. pp. 1971–1980 (2021)
11. ROUGE, L.C.: A package for automatic evaluation of summaries. In: Proceedings of Workshop on Text Summarization of ACL, Spain. vol. 5 (2004)
12. Tanida, T., Müller, P., Kaissis, G., Rueckert, D.: Interactive and explainable region-guided radiology report generation. In: Proceedings of the IEEE/CVF Conference on Computer Vision and Pattern Recognition. pp. 7433–7442 (2023)
13. Vedantam, R., Lawrence Zitnick, C., Parikh, D.: Cider: Consensus-based image description evaluation. In: Proceedings of the IEEE conference on computer vision and pattern recognition. pp. 4566–4575 (2015)
14. Yao, L., Wang, W., Jin, Q.: Image difference captioning with pre-training and contrastive learning. In: Proceedings of the AAAI Conference on Artificial Intelligence. vol. 36, pp. 3108–3116 (2022)
15. Ye, W., Yao, J., Xue, H., Li, Y.: Weakly supervised lesion localization with probabilistic-cam pooling. arXiv preprint arXiv:2005.14480 (2020)